Experimental determination of the optimum working conditions of a transcritical CO_2 refrigeration plant with integrated mechanical subcooling.

Laura Nebot-Andrés*, Jesús Catalán-Gil, Daniel Sánchez, Daniel Calleja-Anta, Ramón Cabello, Rodrigo Llopis

Thermal Engineering Group, Mechanical Engineering and Construction Department,
Jaume I University, Spain

*Corresponding author: lnebot@uji.es, +34 964 718133

Abstract

Subcooling methods for transcritical CO_2 plants are being studied in order to improve their behaviour. Among them, the Integrated Mechanical Subcooling system is one of the most promising owing that performs with high efficiency and it is a total-CO_2 system.

This work presents the experimental determination of the optimum working conditions of a transcritical CO_2 plant working with an integrated mechanical subcooling system. The plant was tested at different pressure and subcooling conditions in order to optimize the COP of the plant and determine the optimal conditions for three ambient temperatures 25.0ºC, 30.4ºC and 35.1ºC and evaporation levels between -15.6ºC and -4.1ºC.

Optimum operating conditions were determined and two correlations are proposed to determine the optimal pressure and subcooling as function the gas-cooler outlet temperature and the evaporation level.

Highlights

- CO_2 refrigeration plant with integrated mechanical subcooling is studied experimentally.
- Optimum operating conditions are determined experimentally.
- Heat rejection temperatures (25.0, 30.4 and 35.1ºC) are tested.
- Evaluated at three evaporating levels between -15.6ºC and -4.1ºC.
- Optimum gas-cooler pressure and subcooling degree correlations are stated.

Keywords

CO_2, Transcritical, Integrated Mechanical Subcooling, COP, Optimum conditions

Nomenclature

COP	coefficient of performance
Cp	specific heat capacity, $kJ \cdot kg^{-1} \cdot K^{-1}$
h	specific enthalpy, $kJ \cdot kg^{-1}$
m	mass flow $kg \cdot s^{-1}$
p	absolute pressure, bar
Pc	power consumption, kW
Q	cooling capacity, kW
SUB	degree of subcooling produced in the subcooler, K
t	temperature, ºC
V	volumetric flow, $m^3 \cdot s^{-1}$

Greek symbols

ε	uncertainty
ρ	density, $kg \cdot m^{-3}$

Subscripts

add	addition
dis	compressor discharge
exp	expansion
expe	experimental
g	glycol
gc	gas-cooler
ims	corresponding to the IMS cycle
in	inlet
inter	interpolated
main	corresponding to the main cycle
0	evaporating level
o	outlet
sub	corresponding to the subcooler
suc	compressor suction
w	water

1. Introduction

Carbon dioxide refrigeration systems have been the centre of effort of many of the scientific research in the recent years. The purpose of these studies was to improve the classical CO_2 systems to make them systems more competent, especially in hot climates. All these efforts have been fostered by the F-Gas Regulation (European Commission, 2014) that limits the use of refrigerants of high GWP in many of today's refrigeration applications. It is necessary to look for refrigerants with low GWP and for certain applications CO_2 is the only candidate with low GWP that ensures safety and it is non-flammable nor toxic (A1 ASHRAE classification).

Although these systems were flatly used in the northernmost countries of Europe due to their good performance in those climates, in southern Europe and other regions of the planet, where the average annual temperature is much higher, these systems suffer a significant decline in their performance.

The use of CO_2 systems with parallel compression was proposed as a way of enhancing the energetic behaviour of these systems. Sarkar and Agrawal (2010) performed the optimization of different architectures with parallel compression and quantified the COP improvements, reaching as maximum 47.3% in optimum COP employing parallel compression economization. Chesi et al. (2014) carried on an experimental study on the parallel compression cycle with flash tank but they do not reach the theoretical values of cooling capacity and COP due to several phenomena that they found in real application.

Another alternative studied in order to upgrade CO_2 systems is the use of ejectors. The latest proposals try to find solutions with variable ejectors such as the multi-ejector (Gullo et al., 2019) or the adjustable ejector (Lawrence and Elbel, 2019).

In addition to the alternatives already mentioned, the use of CO_2 in warm climates has been considered in cascade systems or combined with the dedicated mechanical subcooling. Nebot-Andrés et al. (2017) studied both alternatives for a warm climate like that of Spain. They concluded that the dedicated mechanical subcooling would offer highest energy efficiencies in overall-year operation for evaporating levels over -15ºC.

Subcooling methods define a clear line of research that is acquiring a lot of weight at this time (Yu et al., 2019). Llopis et al. (2018) compiled in a general way the effects of subcooling on CO_2 cycles and reviewed all the methods existing up to the moment to generate this subcooling and sum up the works done so far. Initially, with the most basic subcooling methods such as the internal heat exchanger (Llopis et al., 2015b), and subsequently with more complex systems such as dedicated mechanical subcooling (DMS). The dedicated mechanical subcooling has been studied in the last years, offering important improvements for CO_2 cycles both in terms of COP and cooling capacity. The first studies, of a theoretical nature, were carried out by Llopis et al. (2015a) who studied a transcritical plant with dedicated mechanical subcooling working with R290 for different evaporation levels and heat rejection temperature. In the obtained results, an optimal working pressure was identified but the optimum subcooling degree was not considered. Despite this, the results showed increases in the overall COP that reached increments in reference to the base system without subcooling of 18.4% for t_0=-30ºC, 17.9% for -5ºC and 12.3% for 5ºC.

The studies that followed this, presented data with optimized pressure and subcooling degree, so that maximum COP conditions were obtained. Dai et al. (2017) studied a R152a DMS single-stage system at optimum conditions, obtaining the most significant improvements for higher ambient temperatures and low evaporation levels, achieving an increment of 25.3% in COP for t_o=0ºC and 30ºC of ambient temperature. They also studied the performance advantages of using zeotropic mixtures in the auxiliary cycle (Dai et al., 2018) concluding that the maximum COP is directly related to the glide of the mixture due to the small heat transfer irreversibility that is generated. They obtained increments of 4.9% in COP by using a R32/R1234ze(Z) (55/45) mixture in the DMS cycle instead of pure R32.

In parallel, this system was also studied from an experimental point of view. First, Llopis et al. (2016) presented the experimentation of a CO_2 plant with and without subcooling (working with R1234yf). These tests were only optimized in terms of discharge pressure because the subcooling degree was not adapted in order to enhance the COP. However, the results presented increments in COP at the evaporation level of 0ºC of 10.9% at 24.0ºC, 22.1% at 30.2ºC and 26.1% at 40.0ºC. In addition, the measured increments in capacity were of 23.1% at 24.0 °C, 34.0% at 30.2ºC and 39.4% at 40.0ºC. Authors also corroborated the reduction of the optimal working pressure, being it reduced up to 8 bar in relation to the system working without DMS. In addition, other experimental tests have been carried out, both for single stage (Sánchez et al., 2016) and booster systems (Beshr et al., 2016; Bush et al., 2017).

The dedicated subcooling cycles have been quite studied in recent years, they being very interesting for the integration with air conditioning systems but they still are a not only-CO_2 system. However, for space heating applications, a combined system using only CO_2 has been studied (Cao et al., 2019). Cao et al.

presented a transcritical CO_2 heat pump combined with a subcooling system working with CO_2, obtaining increments of 15.3% in COP comparing to the standard transcritical CO_2 heat pump systems.

The integrated mechanical subcooling cycle (IMS), presented on this paper, only uses CO_2 as refrigerant for refrigeration applications. The purpose of this system is to subcool the CO_2 at the exit of the gas cooler thanks to a part of the current that is extracted from the main cycle and expanded, passing through the subcooler and recompressed until the gas-cooler entrance. The extraction of the CO_2 can be done from the exit of the gas-cooler, the exit of the subcooler and the liquid tank. The interest of this cycle is that it is simpler than the dedicated; it has fewer components, and only works with CO_2. As well as the dedicated does, this subcooling cycle produces large increments in cooling capacity and COP with respect to the base cycle (Catalán-Gil et al., 2019).

The IMS system was firstly proposed by the patent of Shapiro (2009). Cecchinato et al. (2009) evaluated the system from a theoretical point of view and obtained an increment of 17.3% in energy efficiency in relation to a basic single-stage CO_2 cycle for an evaporating level of −10°C of and a gas-cooler outlet temperature of 30°C. This cycle has certain similarities with the one presented by Sarkar and Agrawal (2010) called parallel cycle with economizer. However, Sarkar and Agrawal's cycle only includes two control elements (two expansion valves) and does not allow to optimize all the degrees of freedom, which is needed for centralized refrigeration systems.

Later, Catalán-Gil et al. (2019) analyzed the thermodynamic models of the integrated mechanical subcooling and the dedicated for CO_2 booster systems for supermarket applications, achieving annual energy consumption reductions from 2.9% to 3.4% for warm zones and from 1.3% to 2.4% for hot regions. Nebot-Andrés et al. (2019a) studies from a theoretical approach the IMS system optimizing gas-cooler pressure and the subcooling degree, reaching increments of 15.9% for −10 °C of evaporation temperature and 35ºC of environment temperature in comparison to the CO_2 cycle with internal heat exchanger studied by Chen and Gu (2005). Subcooled boosters have also been studied for space heating by Song et al. who evaluated the optimal discharge pressure for these cycles (Song et al., 2018) and the optimal medium temperature (Song and Cao, 2018).

The integrated mechanical subcooling represents an important interest for the enhancement of CO_2 cycles, having a strong potential of improvement. However, this cycle has never been tested experimentally and its optimum conditions have not been determined or studied, to the knowledge of authors.

Accordingly, this work has been developed in order to determine experimentally the optimum conditions, in terms of subcooling degree and gas-cooler pressure, of an integrated mechanical subcooling system of a CO_2 refrigeration plant, working in transcritical conditions. The main objective is to identify the existence of these optimal conditions, determine which are the needed values to obtain the best results in terms of COP and to define an expression that generalizes the optimum pressure and optimum subcooling degree for this type of systems. The results presented on this paper correspond to the evaluation of a single – stage plant at different evaporation levels, maintaining the temperature of the secondary fluid at the entrance of the evaporator (-1.3ºC, 3.8ºC and 10.0ºC) and three heat rejection temperatures (25.0ºC, 30.4ºC and 35.1ºC), determining for each test the optimum value of pressure and subcooling degree.

The optimum conditions have been determined and stated on a general correlation depending on the evaporation temperature and the temperature at the exit of the gas-cooler. The evolution of the main energy parameters is analyzed as well as the behavior of the optimum conditions of pressure and subcooling degree.

2. Refrigeration cycle and description of the experimental plant

This section presents the experimental installation used to evaluate the optimal conditions of the CO_2 transcritical cycle with the integrated mechanical subcooling system. The most important details of the main components of the cycle are provided and the measurement system used in the plant is described.

2.1. Experimental plant

The experimental plant tested in this work is shown in Figure 1 and its scheme in Figure 2. The plant is a CO_2 single-stage transcritical refrigeration system with an integrated mechanical subcooling system extracting gas at the exit of the subcooler. The main single-stage refrigeration cycle uses a semihermetic compressor with a displacement of 3.48 $m^3 \cdot h^{-1}$at 1450 rpm and a nominal power of 4 kW. The expansion is carried out by a double-stage system, composed of an electronic expansion valve (back-pressure) controlling the gas-cooler pressure, a liquid receiver between stages and an electronic expansion valve, working as thermo-static, to control the evaporating process. Evaporator and gas-cooler are brazed plate counter current heat exchangers with exchange surface area of 4.794 m^2 and 1.224 m^2, respectively. The subcooler is situated directly downstream of the gas-cooler. It is a brazed plate heat exchanger with an exchange surface area of 0.850 m^2. It works as evaporator of the mechanical subcooling system and subcools the CO_2 at the exit of the gas-cooler. The mechanical subcooling cycle is driven by a variable speed semihermetic compressor with displacement of 1.12 $m^3 \cdot h^{-1}$ at 1450 rpm. The expansion valve of the IMS cycle is electronic, working as thermostatic.

Heat dissipation in gas-cooler is done with a water loop, simulating the heat rejection level. The evaporator is supplied with another loop, working with a propylene glycol–water mixture (60% by volume) that enables a constant entering temperature in the evaporator. Both the mass flow and the inlet temperature are controlled in these loops.

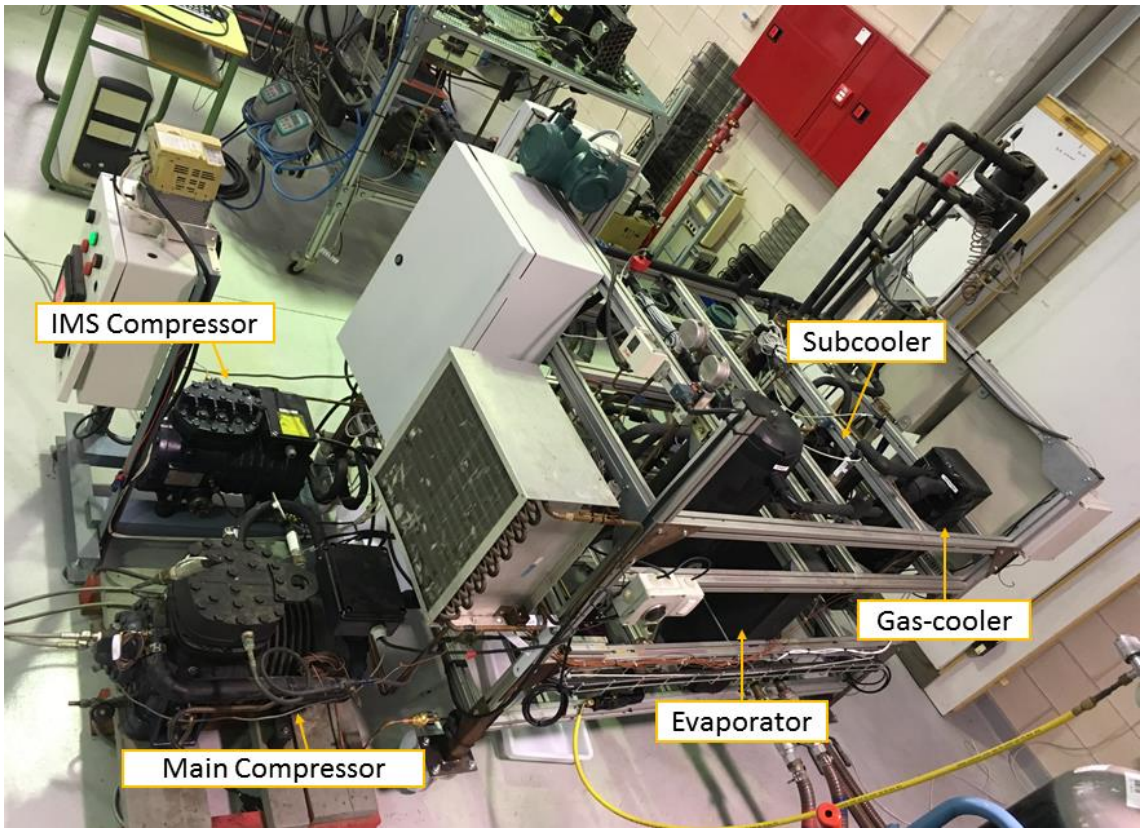

Figure 1. Experimental plant

2.2. Measurement system

The thermodynamic properties of the working fluids are obtained thanks to the measurement system presented in Figure 2. All fluid temperatures are measured by 18 T-type thermocouples. The thermocouples placed at the evaporator and at the exit of gas-cooler and subcooler are immersion thermocouples. 11 pressure gauges are installed along all the circuit. CO_2 mass flow rates are measured by two Coriolis mass flow meters, as well as dissipation water flow of the gas-cooler, which is measured using another one. The flow of the other secondary fluids is measured by a magnetic volumetric flow meter. Compressors' power consumptions are measured by two digital wattmeters. The accuracies of the measurement devices are presented in Table 1.

Table 1. Accuracies and calibration range of the measurement devices.

Measured variable	Measurement device	Range	Calibrated accuracy
Temperature (ºC)	T-type thermocouple	-40.0 to 145.0	±0.5K
CO_2 pressure (bar)	Pressure gauge	0.0 to 160.0	±0.6% of span
CO_2 pressure (bar)	Pressure gauge	0.0 to 100.0	±0.6% of span
CO_2 pressure (bar)	Pressure gauge	0.0 to 60.0	±0.6% of span
CO_2 main mass flow rate ($kg \cdot s^{-1}$)	Coriolis mass flow meter	0.00 to 1.38	±0.1% of reading
CO_2 IMS mass flow rate ($kg \cdot s^{-1}$)	Coriolis mass flow meter	0.00 to 0.083	±0.1% of reading
Water mass flow rate ($kg \cdot s^{-1}$)	Coriolis mass flow meter	0.00 to 13.88	±0.1% of reading
Glycol volume flow rate ($m^3 \cdot h^{-1}$)	Magnetic flow meter	0.0 to 4.0	±0.25% of reading
Power consumption (kW)	Digital wattemeter	0.0 to 6.0	±0.5% of reading

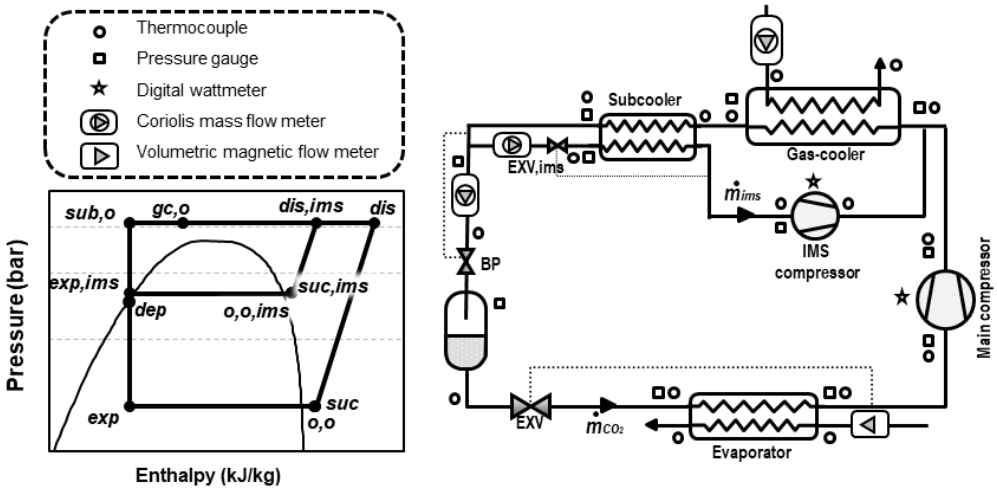

Figure 2. Schema of the experimental plant and the measurement system and Ph diagram of the cycle.

3. Experimental tests

This section contains the description of the strategy for conducting the experimental tests in order to determine the optimum conditions of the cycle for different heat rejection levels and different evaporation temperatures.

3.1. Test procedure

To evaluate the refrigeration plant using integrated mechanical subcooling, the system has been tested at different working conditions always operating in the transcritical region. The evaluated conditions were:

- Heat rejection level: three different temperatures: 25.0, 30.4 and 35.1°C, with maximum deviation of ±0.20°C. These levels were performed fixing the temperature of the secondary fluid (water) at the entrance of the gas-cooler and maintaining the water flow rate to 1.167 $m^3 \cdot h^{-1}$.

- Three different evaporation levels maintaining the inlet temperature of the secondary fluid in the evaporator and the flow rate. The secondary fluid is a mixture propylene glycol-water (60% by volume) and the evaluated temperatures were -1.3±0.07°C, 3.8±0.12°C and 10.1±0.23°C. The flow rate was fixed to 0.7 $m^3 \cdot h^{-1}$.

- Gas-cooler pressure was regulated with an electronic BP fixed during each test thanks to a PDI controller. Each test was performed at different pressures in order to identify the optimum one and reach the optimum COP conditions.

- Compressors: The main compressor always operated at nominal speed of 1450 rpm. The speed of the IMS compressor was varied is order to obtain the optimum subcooling degree.

- Electronic expansion valves: The electronic expansion valves were set to obtain a superheating degree in the evaporator of 10K and of 5K on the subcooler.

All the tests were carried out in steady state conditions for periods longer than 10 minutes, taking data each 5 seconds, obtaining the test point as the average value of the whole test. The measured data were used to calculate the thermodynamic properties of the points using Refprop v.9.1. (Lemmon et al., 2013).

3.2. Test range

Table 2 sumps up all the tests carried out, including the number of tests performed in each of the evaluated conditions. The range of values evaluated for the subcooling degree, the gas-cooler pressure and the main energy parameters for each test are also detailed on it.

Table 2. Experimental tests and range of tested conditions.

$t_{w,in}$ (ºC)	$t_{g,in}$ (ºC)	number of tests	SUB (K)	p_{gc} (bar)	COP (-)	Q_0 (kW)
25.0	-1.3	8	19.4-23.4	74.0-75.0	1.77-1.83	7.4-7.7
	3.8	8	16.1-21.4	74.5-76.0	2.02-2.12	8.7-8.9
	10.1	21	8.8-19.7	74.0-78.1	2.49-2.96	11.3-12.1
30.4	-1.3	17	10.7-24.3	78.9-89.3	1.48-1.60	6.4-7.2
	3.8	23	11.8-23.6	80.0-91.9	1.47-1.82	7.8-8.4
	10.1	19	8.6-16.2	80.2-82.2	1.92-2.10	9.1-9.6
35.1	-1.3	23	18.5-25.6	86.9-89.3	1.29-1.38	6.3-6.5
	3.8	18	3.8-18.5	84.0-90.9	1.40-1.58	6.1-7.6
	10.1	18	3.6-12.7	85.1-90.9	1.66-1.84	7.6-8.8

4. Optimization of the plant

In transcritical refrigeration cycles with subcooling there is an optimum working condition where the COP is maximum (Llopis et al., 2018). This point corresponds to the optimal gas-cooler pressure and the optimal subcooling degree, defined as eq. (1). The subcooling degree is the difference between the temperature at the exit of the gas-cooler and the temperature at the exit of the subcooler. The tests were carried out in order to demonstrate the existence of this optimum, identify it, and then to evaluate the behaviour of the plant at optimum conditions.

$$SUB = t_{gc,o} - t_{sub,o} \quad (1)$$

4.1. Experimental COP identification

The cooling capacity of the plant is calculated as the product of the mass flow rate through the evaporator ($\dot{m}_{co2}$) and the enthalpy difference in evaporator, as shown in Eq. (2). The enthalpy at the evaporator inlet ($h_{0,o}$) is considered to be the same as the enthalpy at the inlet of the back-pressure valve. The COP of the system is the ratio between the cooling capacity and the sum of the power consumption of two compressors, as established in Eq. (3).

To obtain the maximum COP, tests have been carried out modifying pressure and subcooling values following a method similar to a Simplex algorithm. When three initial points were available, these parameters were increased or decreased following the trend of the previous points, in order to get closer and closer to the point of maximum COP. The process ended when the increments achieved between the new value and the previous one were less than 1%.

$$\dot{Q}_0 = \dot{m}_{co2} \cdot \left(h_{0,o} - h_{exp}\right) \quad (2)$$

$$COP = \frac{\dot{Q}_0}{P_{C,main} + P_{C,ims}} \quad (3)$$

Figure 3 shows the measured COP for the tested condition of $t_{w,in}$ = 35.1ºC and $t_{g,in}$ = 10.0ºC, for different pressure levels and several subcooling degrees, representing the value of the COP as a function of Pgc and SUB. This colour map shows the evolution of the COP, where the existence of a maximum COP is clearly observed. Reducing or increasing pressure or subcooling degree will always reduce the obtained value of COP. As it can be seen, the influence of the pressure on the variation of the COP is higher than the influence of the subcooling degree. Increasing or reducing the pressure 1.5% has a higher impact on the COP than modifying the subcooling degree in the same percentage.

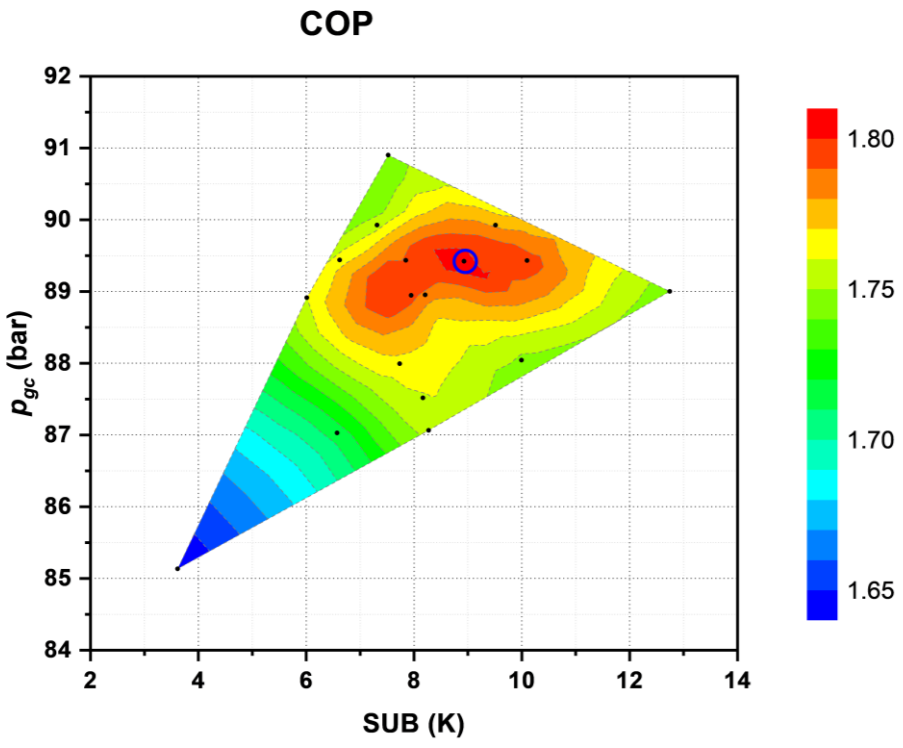

Figure 3. Experimental COP for $t_{w,in}$ = 35.1ºC and $t_{g,in}$ = 10.0ºC.

4.2. Experimental analysis of the cooling capacity

Regarding cooling capacity, calculated with Eq. (2), the subcooling degree increases the capacity of the plant, it being higher when higher the subcooling degree is, as it can be seen in Figure 4. Due to that, the optimum condition does not correspond to the point with higher cooling capacity, but the difference is not remarkable. The positive aspect of this effect is that the capacity of the system can be adjusted by modifying the subcooling degree in order to fit the needs of the application with decrements in COP of 1.5% when increasing or decreasing 2K of subcooling.

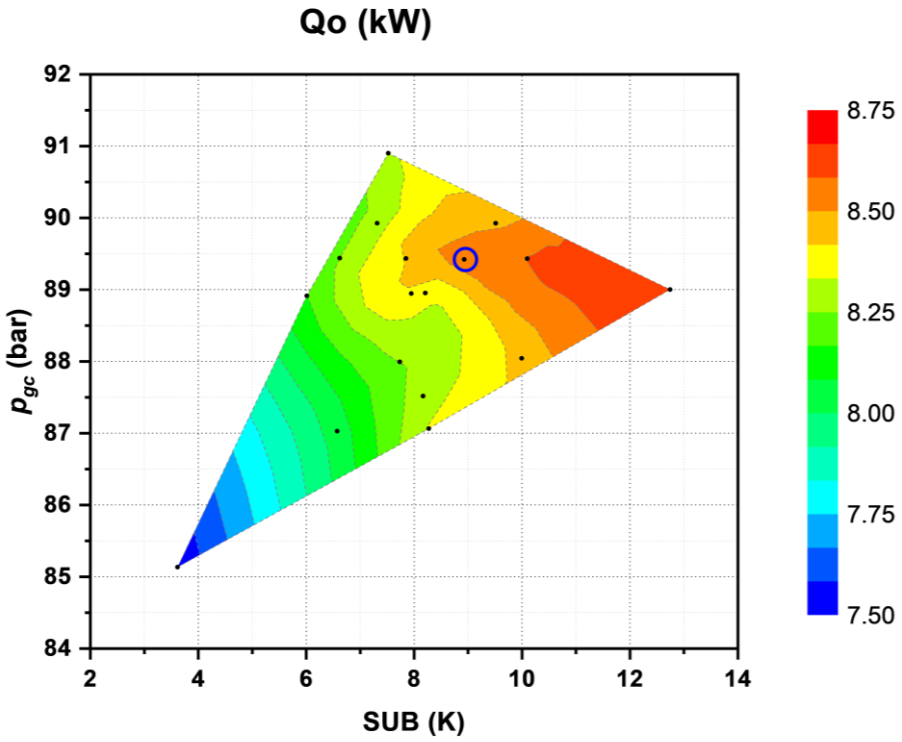

Figure 4. Experimental cooling capacity for $t_{w,in}$ = 35.1ºC and $t_{g,in}$ = 10.0ºC.

4.3. Optimum COP evaluation

Even it is not possible to determine with exactitude the exact value of the optimum COP, the experimental tests have allow to identify the region where the maximum COP is. To obtain the exact optimum COP, an interpolation of all the experimental data has been carried out. For that, all the measured values have been taken into account and referred to the subcooling degree and the gas-cooler pressure.

The data has been interpolated using the method of thin-plate spline (Bookstein, 1992), obtaining a 3D representation of the behaviour of the COP depending on the working pressure and the subcooling degree. Then, the interpolated function has been used to determine the exact position of the optimum COP values. The optimum COP values for the entire evaluation range are presented in Table 3, as well as the difference between this value and the maximum COP registered experimentally.

Figure 5 shows the interpolation at $t_{w,in}$=25.0ºC and $t_{g,in}$=1.3ºC. The blue points represent the measured experimental points and the red point represents the optimum point, obtained by the interpolation. The difference between the experimental and the interpolated point, calculated with Eq. (4), is 0.34% in

average and a maximum difference of 1.46% at one of the tested conditions, which means that the maximum point obtained experimentally is practically the same as the obtained by the interpolation.

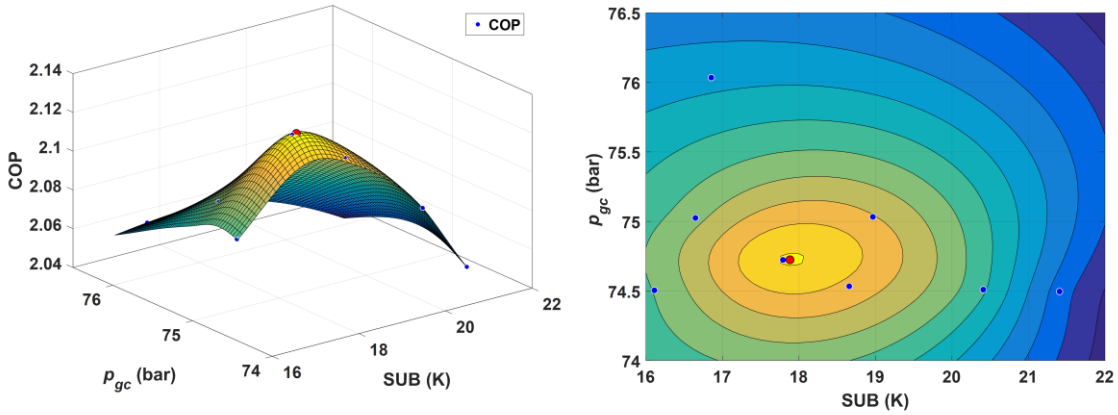

Figure 5. 3D and contour thin-plate spline interpolation of the COP at $t_{w,in}$=25.0ºC and $t_{g,in}$=-1.3ºC

$$\Delta COP\ (\%) = \frac{COP_{inter} - COP_{expe}}{COP_{expe}} \cdot 100 \qquad (4)$$

Table 3. Experimental data vs interpolated results.

		Experimental data	Thin-plate spline	
Tw,in (ºC)	Tgly,in (ºC)	COP (-)	COP (-)	ΔCOP (%)
25.2	-1.4	1.866	1.868	0.11
30.5	-1.3	1.626	1.626	0.02
35.0	-1.3	1.404	1.409	0.36
25.0	3.7	2.131	2.131	0.01
30.4	3.8	1.818	1.822	0.20
35.2	3.9	1.564	1.578	0.92
24.8	9.9	2.482	2.482	0.01
30.2	9.9	2.101	2.132	1.46
35.1	10.3	1.811	1.811	0.00

5. Experimental results at optimum conditions

The results presented in this section correspond to the tests where the COP is maximum for each evaluated condition. The presented results are the measured data and not the interpolated due to the minimal difference between them, as discussed in the previous section. Figure 6 represents the working cycle of the refrigeration system, with the most important points of measure. The red points correspond to the test conditions with the inlet glycol temperature of 10.0ºC, the green ones to the 3.8ºC and the blue ones to the -1.3ºC. The drawn cycles correspond to the water inlet temperature of 30.4ºC. For water temperatures of 25.0ºC and 35.1ºC, only the points of the exit of the gas-cooler and subcooler exit are represented.

As it can be seen, at the water temperature level of 30.4ºC, the three gas-cooler exit points, corresponding to the three evaporation levels, are practically coincident, having them all very similar approach of temperature at gas-cooler. However, the subcooler exit points are not the same. Thus, here it is possible to observe the different optimum subcooling degree needed for each evaporation level since the subcooler

outlet point is farther from the gas-cooler outlet when lower the evaporation temperature is. The same phenomenon is repeated at the water inlet temperature levels of 25.0ºC and 35.1ºC. In the diagram, it can also be observed that for a water inlet temperature condition, there is no large difference in terms of high pressure for the different evaporation levels, so the optimum gas-cooler pressure is slightly dependent on the evaporation temperature.

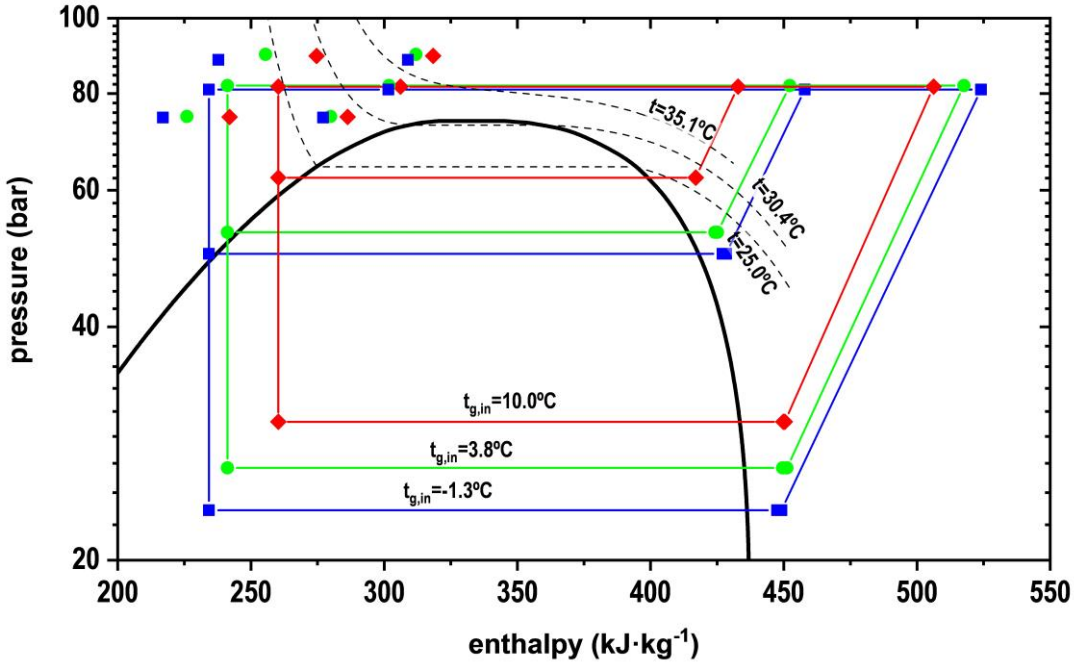

Figure 6. P-h diagram of the cycle at optimum working conditions for all the tests.

Table 4 sums up the main results. It contains the optimum COP of each tested condition, the main temperatures, the cooling capacity and power consumption of the compressors as well as the uncertainty and the energy balances for data validation. COP, cooling capacity and working conditions are discussed in the following subsections.

The main energy parameters studied in this work are cooling capacity and COP, defined by Eq.(2) and Eq.(3), respectively. The uncertainty of these main parameters has been calculated using Moffat's method (Moffat, 1985) and the measurement devices' accuracies. The average measured uncertainty is ±0.85% in $\dot{Q}_0$ and ±0.95% in COP. The uncertainty ε(COP) and ε(Q_0) of all the results presented in this work is compiled in Table 4. To ensure correct measurement of the parameters in the cycle, the energy balances in evaporator, gas-cooler and subcooler have been calculated taking into account the capacity transmitted on the CO_2 side and on the secondary fluid.

Eq. (5) is the heat transfer at the side of the glycol. Eq. (6) quantifies the discrepancy between the heat transfer of the glycol and the cooling capacity on the evaporator.

$$\dot{Q}_g = \dot{V}_g \cdot \rho_g \cdot Cp_g \cdot (t_{g,in} - t_{g,o}) \quad (5)$$

$$\Delta\dot{Q}_{evap} = \frac{\dot{Q}_0 - \dot{Q}_g}{\dot{Q}_0} \cdot 100 \quad (6)$$

Eq. (7) corresponds to the heat transfer of the CO_2 in the gas-cooler and Eq. (8) in the water side. The difference between the heat transfers of each of the fluids is calculated as Eq. (9).

$$\dot{Q}_{gc} = (\dot{m}_{co2} + \dot{m}_{ims}) \cdot (h_{gc,in} - h_{gc,o}) \quad (7)$$

$$\dot{Q}_w = \dot{V}_w \cdot \rho_w \cdot C_{p,w} \cdot (t_{w,in} - t_{w,o}) \quad (8)$$

$$\Delta\dot{Q}_{gc} = \frac{\dot{Q}_{gc} - \dot{Q}_w}{\dot{Q}_{gc}} \cdot 100 \quad (9)$$

The capacity of the subcooler is calculated as Eq. (10) for the side corresponding to the CO_2 subcooled and Eq. (11) corresponds to the cooling capacity of the subcooler for the evaporation fluid. The heat transfer difference between both sides of the subcooler is calculated as Eq. (12).

$$\dot{Q}_{sub} = (\dot{m}_{co2} + \dot{m}_{ims}) \cdot (h_{gc,o} - h_{sub,o}) \quad (10)$$

$$\dot{Q}_{0,sub} = \dot{m}_{ims} \cdot (h_{sub,o} - h_{0,o,ims}) \quad (11)$$

$$\Delta\dot{Q}_{sub} = \frac{\dot{Q}_{0,ims} - \dot{Q}_{sub}}{\dot{Q}_{0,ims}} \cdot 100 \quad (12)$$

These balance differences are presented in Table 4. As it can be seen, the differences are quite small: 3.4% at evaporator in average, 3.8% at gas-cooler and 5.2% at subcooler. In tests number E3, E4 and E6 the discrepancies are greater than 5%. This is because the gas-cooler outlet is near the pseudocritical region where due to the variation of the isobaric heat capacity, small changes in temperature result in high measurement uncertainties (Torrella et al., 2011).

5.1. Maximum COP

Figure 7 shows the evolution of the maximum measured COP for all the evaluated conditions. It can be seen a clear trend in its evolution, marked by the glycol and the water inlet temperatures. For all the glycol levels, it can be perceived that the COP is lower when lower the glycol inlet temperature is, so when lower the evaporation level is. It can be also observed that, as the water inlet temperature increases (corresponding to the heat rejection level) the COP decreases, so lower COPs are obtained when higher is the heat rejection temperature.

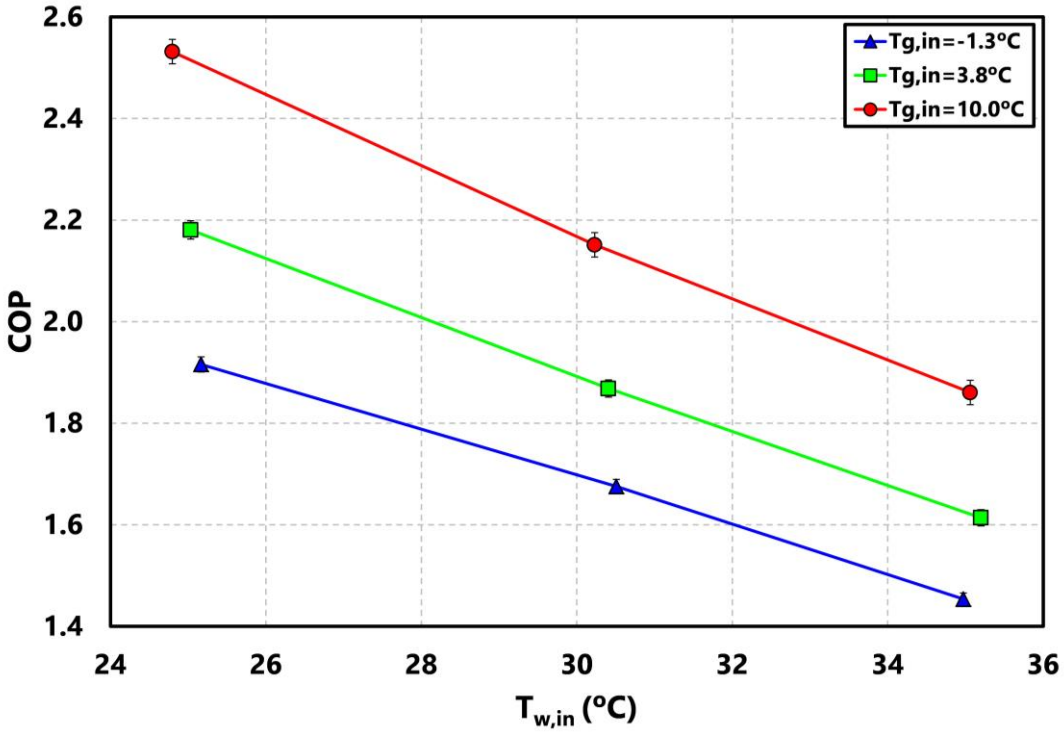

Figure 7. Evolution of the maximum COP for optimal conditions depending on the water inlet temperature.

The measured values go from 1.40 to 1.87 for $t_{g,in}$ = -1.3ºC, from 1.56 to 2.13 for $t_{g,in}$ = 3.8ºC and from 1.81 to 2.48 for $t_{g,in}$ = 10.0ºC.

5.2. Cooling capacity

The cooling capacity that the plant is capable of providing under the conditions of maximum COP is represented in Figure 8. A linear trend can be observed depending on the heat rejection temperature, reducing the cooling capacity of the plant as the water inlet temperature increases. Likewise, it is clearly observed how the capacity is greater when higher the evaporation level is.

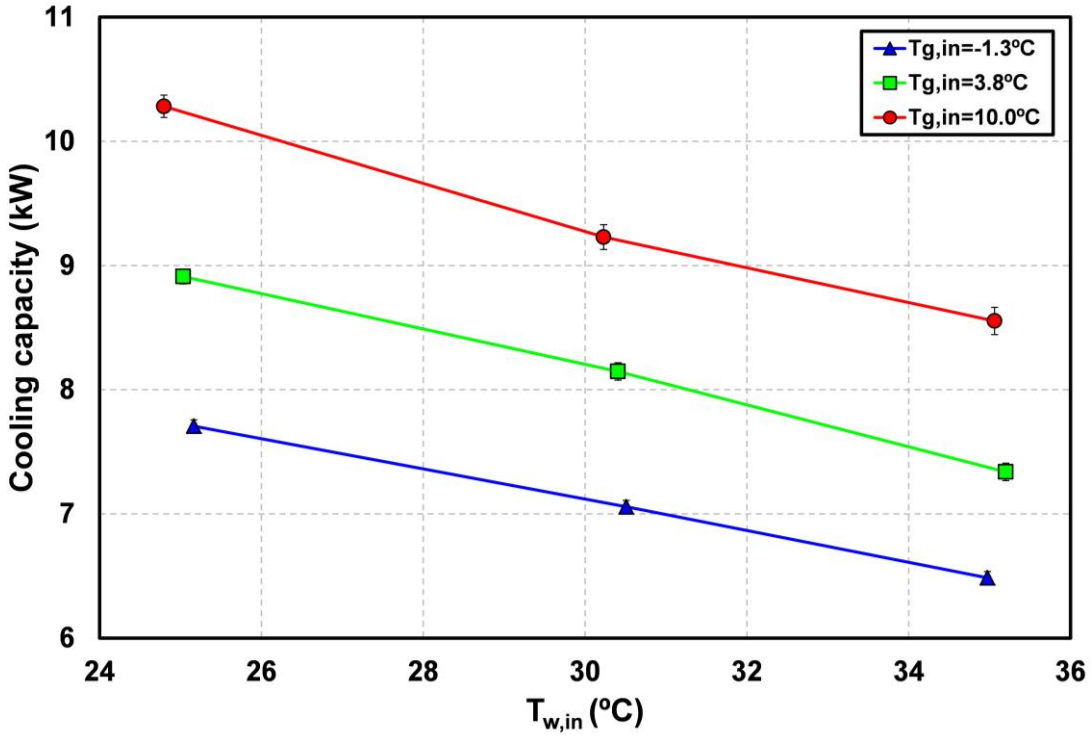

Figure 8. Evolution of the cooling capacity for optimal conditions depending on the water inlet temperature.

The measured values go from 6.5kW to 7.7kW for $t_{g,in}$ = -1.3ºC, from 7.3kW to 8.9kW for $t_{g,in}$ = 3.8ºC and from 8.6kW to 10.3kW for $t_{g,in}$ = 10.0ºC.

Cooling capacity can also be described as shown in Eq. (13), where the first term corresponds to the cooling capacity if there was not subcooling and the second to the contribution generated by the subcooling cycle. So the cooling capacity of the system can be defined as the sum of two terms, as shown by Eq. (14), the capacity of the system without subcooling ($\dot{Q}_{base}$) and the capacity added by the subcooler, Eq. (15).

$$\dot{Q}_0 = \dot{m}_{co2} \cdot \left(h_{0,o} - h_{gc,o}\right) + \dot{m}_{co2} \cdot \Delta h_{sub} \quad (13)$$

$$\dot{Q}_0 = \dot{Q}_{base} + \dot{m}_{co2} \cdot \Delta h_{sub} \quad (14)$$

$$\dot{Q}_{sub,add} = \dot{m}_{co2} \cdot \Delta h_{sub} \quad (15)$$

The proportion of the cooling capacity corresponding to the contribution of the subcooler represents in all cases less than a third of the total cooling capacity and goes from 2.0kW to 2.4kW. This contribution is greater the higher the water temperature and the lower the evaporation level are (when further the heat source and hot sink are). The effect of the subcooling cycle is higher at high rejection temperatures and low evaporation levels because these are the conditions where the behaviour of the plant needs to be more improved due to the reduction of the COP, as it was presented by Nebot-Andrés et al. (2019b). The

contributions represent between 25.6% and 21.5% at 25.0ºC, between 31.5% and 24.1% at 30.4ºC and between 33.2 and 24.9 at 35ºC.

Figure 9 shows the total cooling capacity of the plant divided into the cooling capacity corresponding to the cycle without subcooling and the subcooling contribution.

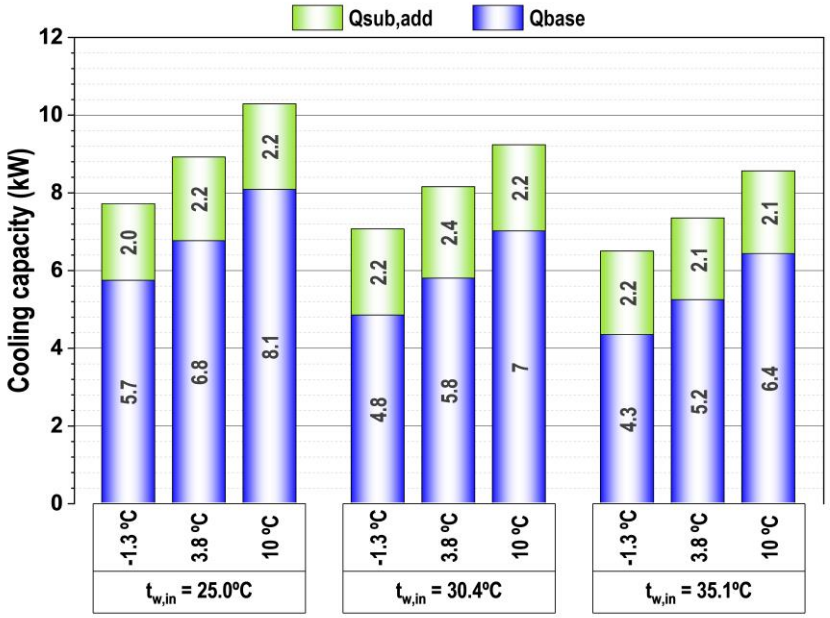

Figure 9. Cooling capacity broken down into base capacity and subcooler contribution.

Figure 10 represents the power consumption of each of the compressors of the plant for the different evaluated conditions. The increment in the power consumption due to the introduction of an additional compressor can be noticed. However, the power consumption of the IMS compressor is much lower than those of the main compressor. In addition, as seen in the previous sections, the cooling capacity is increased in higher proportions, thus this effect is positive for the overall COP of the plant.

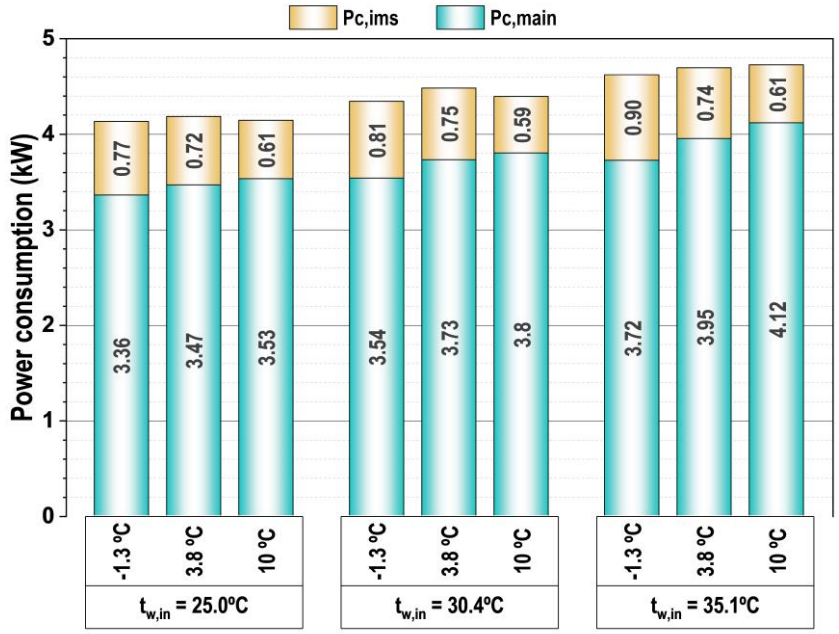

Figure 10. Power consumption of each of the compressors.

5.3. Optimum pressure

Figure 11 shows the optimum gas-cooler pressure value for each test condition. It can be observed that for the three glycol temperatures, the evolution of the pressure follows the same trend and also it practically does not depend on the inlet temperature at the evaporator. However, it is clearly correlated with the heat rejection level.

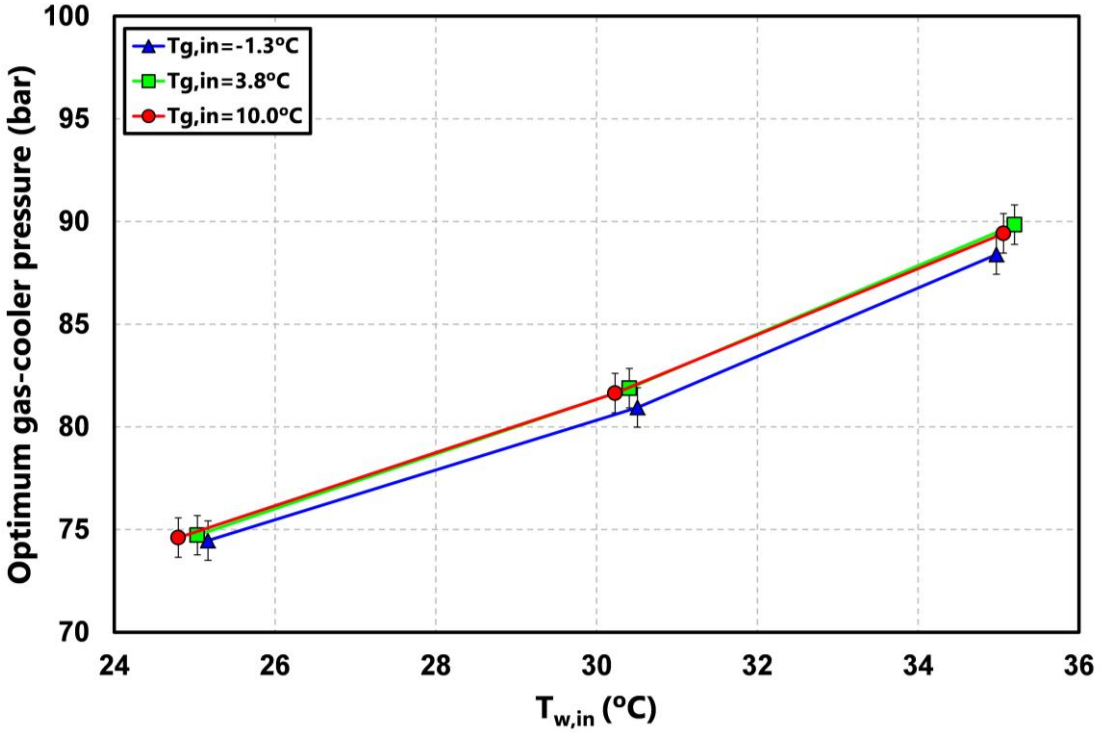

Figure 11. Optimum working pressure for the tested conditions.

There is a small difference for the lower glycol level but this difference is within the limits of the measurement uncertainty, therefore we can state that the optimum pressure depends more strongly on the heat rejection temperature than on the inlet temperature at the evaporator of the plant. Analyzing the influence of the heat rejection level, we can affirm that the higher the temperature is, the greater the pressure of the plant must be.

5.4. Optimum subcooling degree

Optimal subcooling degree is presented in Figure 12. We can affirm that when lower is the evaporation level, greater the degree of subcooling necessary to achieve the optimum COP must be. Analysing each of the different evaporation levels, a slight decreasing trend can be seen for the higher inlet glycol temperatures ($t_{g,in}$ = 3.8ºC and 10.0ºC) while for -1.3ºC the optimal subcooling degree decreases and then increases again. This change in trend in the evolution of the optimal subcooling degree may be because the gas-cooler outlet is near the pseudocritical zone, where CO_2 present abrupt changes in its thermophysical properties. Also, this effect was observed in the theoretical simulations presented by Nebot-Andrés et al. (2017)

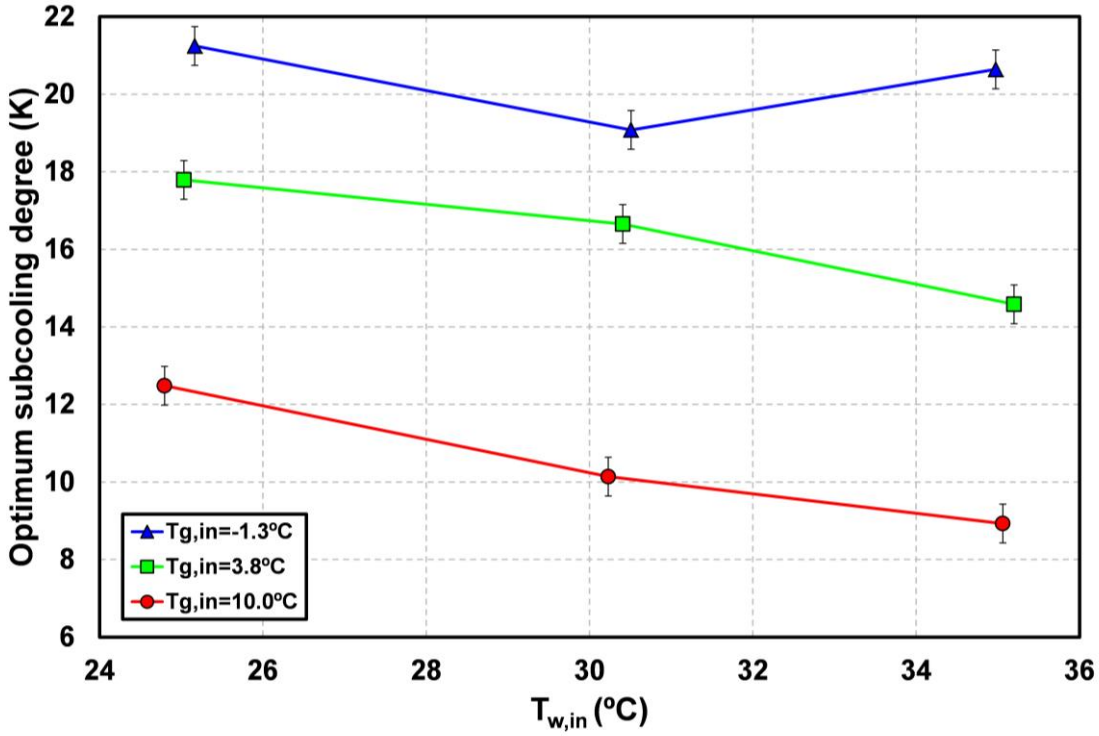

Figure 12.Evolution of the optimum subcooling degree for the tested conditions.

5.5. Correlations

In the previous sections all the results are referred to the inlet water and glycol temperatures because these were the parameters set in the test. In order to generalize more the results, in this section the optimal operating conditions are referred to the evaporation temperature and the gas-cooler outlet temperatures.

The following correlations allow calculating the optimum subcooling degree and the optimal gas-cooler pressure. They have been obtained by adjusting the values obtained experimentally by an adjustment of least-squares.

5.5.1. Optimum pressure

Equation (16) defines the optimum gas-cooler pressure as a function of the evaporation temperature and the gas-cooler outlet temperature.

$$p_{gc} = 126.5 + 0.285 \cdot t_0 - 4.537 \cdot t_{gc,o} - 0.01374 \cdot t_0 \cdot t_{gc,o} + 0.09409 \cdot t_{gc,o}^2 \quad (16)$$

$$27.5ºC \leq t_{gc,o} \leq 37.5ºC$$

$$-15.6ºC \leq t_0 \leq -4.1ºC$$

The range of application of this correlation is for temperatures of gas-cooler exit between 27.5ºC and 37.5ºC and evaporation temperatures between -15.6ºC and -4.1ºC. The average error of this correlation is ±0.3 bar and the maximum error ±0.6 bar.

Kauf (1999), Liao et al. (2000) and Sarkar et al. (2004) proposed correlations to determine the optimum pressure for single-stage transcritical CO_2 cycles. Then, Chen and Gu (2005) proposed a correlation for transcritical carbon dioxide cycles with internal heat exchanger that provide similar results to Kauf's

correlation. Also, Song et al. (2018) presented a correlation based on experimental data to obtain the optimum pressure for subcooler-based transcritical CO_2 systems used as heat pump.

Figure 13 shows the optimum CO_2 gas-cooler pressure based on the different correlations for an evaporating level of -5ºC including the previous correlation presented in eq. (16). Kauf's correlation is not included because the range of application is different. It can be observed that the correlation proposed in this paper provides lower pressures for temperatures over 32ºC at the exit of gas-cooler, corroborating the optimal pressure reduction achieved with the use of subcooling cycles (Dai et al., 2018; Llopis et al., 2016).

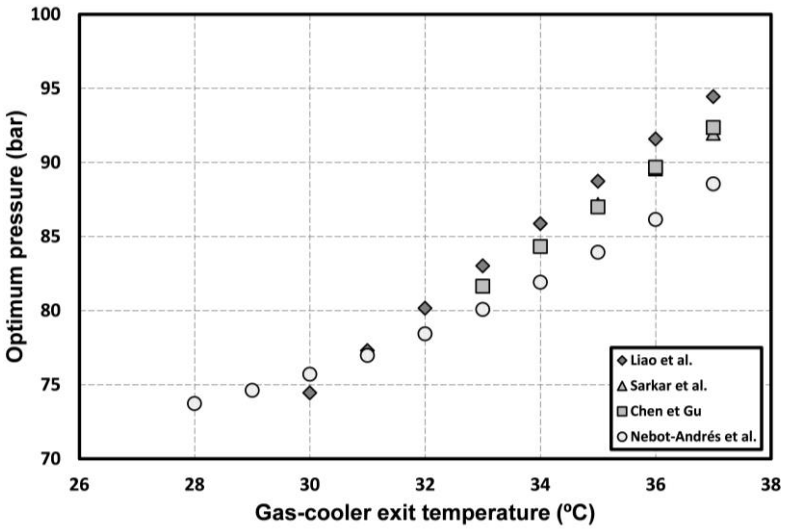

Figure 13. Optimum gas-cooler pressure based on different correlations (t_o=-5ºC).

Figure 14 shows the reduction in pressure obtained comparing the correlation of eq. (16) with the correlations of Liao, Sarkar and Chen. The optimum pressure of the CO_2 system with IMS is gradually reduced when higher the gas-cooler outlet temperature is, compared to a pure transcritical CO_2 cycle. A reduction of 5.9 bar is obtained for $t_{gc,o}$ = 37°C comparing to Liao's correlation. Comparing to Sarkar's expression, an average reduction of 3.3 bar is accomplished for temperatures between 35 and 37ºC. The IMS cycles also reduces the pressure of the system comparing it to cycles with internal heat exchanger, up to -3.8 bar for $t_{gc,o}$ = 37°C.

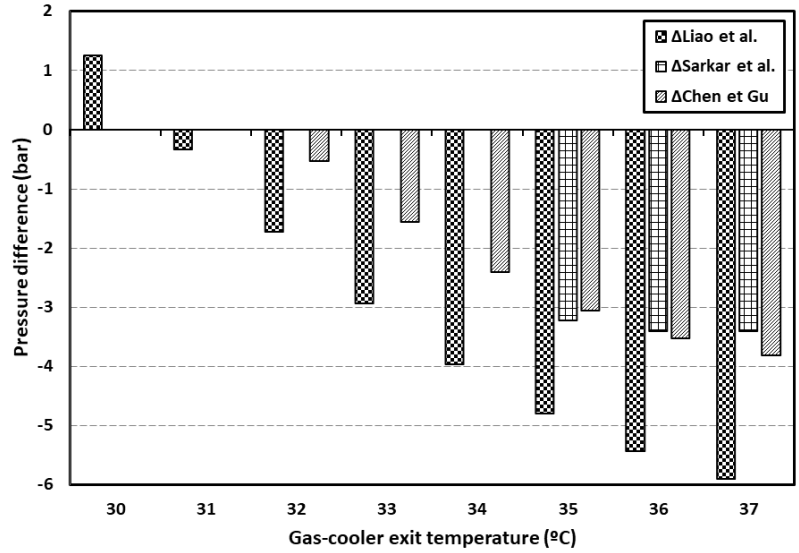

Figure 14. Pressure difference obtained using the IMS optimum pressure correlation.

The correlations posed by the previous authors differ significantly from the optimal pressure of the transcritical cycle with IMS; therefore, the use of the correlation in the eq. (16) is recommended for this type of cycles.

5.5.2. Optimum subcooling degree

Equation (17) shows the correlation between the evaporation temperature and the gas-cooler outlet temperature that defines the optimum subcooling degree needed to obtain the maximum COP when working at the optimum pressure for a CO_2 cycle with integrated mechanical subcooling.

$$SUB = 9.682 - 0.9938 \cdot t_0 - 0.1226 \cdot t_{gc,o}$$
$$27.5ºC \leq t_{gc,o} \leq 37.5ºC \quad (17)$$
$$-15.6ºC \leq t_0 \leq -4.1ºC$$

The range of application of this correlation is for temperatures of gas-cooler exit between 27.5ºC and 37.5ºC and for evaporating levels between -15.6ºC and -4.1ºC. The average error of this correlation is ±0.6K and the maximum error ±1.0K.

6. Conclusions

This paper presents for the first time the experimental optimization of a CO_2 transcritical refrigeration plant with integrated mechanical subcooling. The evaluation covered the heat rejection levels of 25.0ºC, 30.4ºC and 35.1ºC and the cold source temperatures of -1.3ºC, 3.8ºC and 10ºC at steady-state conditions. The main compressor was run at nominal speed while the velocity of the auxiliary compressor was modified in order to obtain the optimum subcooling degree. All the experimental data have been validated by comparing the energy balances in all the heat exchangers of the plant.

The experimental tests have allowed to demonstrate the existence of a maximum COP, obtained at optimum conditions of pressure and subcooling degree. All the tests were performed to obtain the optimal COP of the plant, that goes from 1.40 to 1.87 at $t_{g,in}$ = -1.3ºC, from 1.56 to 2.13 for $t_{g,in}$ = 3.8ºC and from 1.81 to 2.48 for $t_{g,in}$ = 10.0ºC and the cooling capacity from 6.5kW to 7.7kW at tg,in = -1.3ºC, from 7.3kW to 8.9kW for tg,in = 3.8ºC and from 8.6kW to 10.3kW for tg,in = 10.0ºC. On the one hand, the optimum pressure is strongly dependent on the gas-cooler outlet temperature, following a linear trend but it practically does not vary depending on the level of evaporation. On the other hand, the optimum subcooling degree is a function of the gas-cooler outlet temperature and the evaporation temperature, the subcooling being always different for each of the working levels, being higher when lower is the evaporation level.

From the experimental data, two general expressions have been stated to determine the optimum pressure and subcooling in this type of installation, only as a function of its evaporation level and the gas-cooler outlet temperature. Optimum pressure correlation differs significantly from the classical equations, so it is advisable to use the correlation presented in this paper for CO_2 transcritical cycles with integrated mechanical subcooling.

Acknowledgements

The authors thank the Ministry of Economy and Competitiveness - Spain (project ENE2014-53760-R.7), the Ministry of Education, Culture and Sports - Spain (grant FPU16/00151) and the Jaume I University (project UJI-B2017-06) for financing this research work.

References

Beshr, M., Bush, J., Aute, V., Radermacher, R., 2016. Steady state testing and modeling of a CO2 two-stage refrigeration system with mechanical subcooler, Refrigeration Science and Technology, pp. 893-900.

Bookstein, F.L., 1992. Principal warps: Thin-plate splines and the decomposition of deformations. IEEE Transactions on Pattern Analysis and Machine Intelligence v, 567-585.

Bush, J., Beshr, M., Aute, V., Radermacher, R., 2017. Experimental evaluation of transcritical CO2 refrigeration with mechanical subcooling. Science and Technology for the Built Environment 23, 1013-1025.

Cao, F., Cui, C., Wei, X., Yin, X., Li, M., Wang, X., 2019. The experimental investigation on a novel transcritical CO2 heat pump combined system for space heating. International Journal of Refrigeration 106, 539-548.

Catalán-Gil, J., Llopis, R., Sánchez, D., Nebot-Andrés, L., Cabello, R., 2019. Energy analysis of dedicated and integrated mechanical subcooled CO2 boosters for supermarket applications. International Journal of Refrigeration.

Cecchinato, L., Chiarello, M., Corradi, M., Fornasieri, E., Minetto, S., Stringari, P., Zilio, C., 2009. Thermodynamic analysis of different two-stage transcritical carbon dioxide cycles. International Journal of Refrigeration 32, 1058-1067.

Chen, Y., Gu, J., 2005. The optimum high pressure for CO2 transcritical refrigeration systems with internal heat exchangers. International Journal of Refrigeration 28, 1238-1249.

Chesi, A., Esposito, F., Ferrara, G., Ferrari, L., 2014. Experimental analysis of R744 parallel compression cycle. Applied Energy 135, 274-285.

Dai, B., Liu, S., Li, H., Sun, Z., Song, M., Yang, Q., Ma, Y., 2018. Energetic performance of transcritical CO2 refrigeration cycles with mechanical subcooling using zeotropic mixture as refrigerant. Energy 150, 205-221.

Dai, B., Liu, S., Sun, Z., Ma, Y., 2017. Thermodynamic Performance Analysis of CO2 Transcritical Refrigeration Cycle Assisted with Mechanical Subcooling, Energy Procedia, pp. 2033-2038.

European Commission, 2014. Regulation (EU) No 517/2014 of the European Parliament and of the Council of 16 April 2014 on fluorinated greenhouse gases and repealing Regulation (EC) No 842/2006.

Gullo, P., Hafner, A., Banasiak, K., Minetto, S., Kriezi, E.E., 2019. Multi-ejector concept: A comprehensive review on its latest technological developments. Energies 12.

Kauf, F., 1999. Determination of the optimum high pressure for transcritical CO2-refrigeration cycles. International Journal of Thermal Sciences 38, 325-330.

Lawrence, N., Elbel, S., 2019. Experimental investigation on control methods and strategies for off-design operation of the transcritical R744 two-phase ejector cycle. International Journal of Refrigeration.

Lemmon, E.W., Huber, M.L., McLinden, M.O., 2013. REFPROP, NIST Standard Reference Database 23, v.9.1. National Institute of Standards, Gaithersburg, MD, U.S.A.

Liao, S.M., Zhao, T.S., Jakobsen, A., 2000. A correlation of optimal heat rejection pressures in transcritical carbon dioxide cycles. Applied Thermal Engineering 20, 831-841.

Llopis, R., Cabello, R., Sánchez, D., Torrella, E., 2015a. Energy improvements of CO2 transcritical refrigeration cycles using dedicated mechanical subcooling. International Journal of Refrigeration 55, 129-141.

Llopis, R., Nebot-Andrés, L., Cabello, R., Sánchez, D., Catalán-Gil, J., 2016. Experimental evaluation of a CO2 transcritical refrigeration plant with dedicated mechanical subcooling. International Journal of Refrigeration 69, 361-368.

Llopis, R., Nebot-Andrés, L., Sánchez, D., Catalán-Gil, J., Cabello, R., 2018. Subcooling methods for CO2 refrigeration cycles: A review. International Journal of Refrigeration 93, 85-107.

Llopis, R., Sanz-Kock, C., Cabello, R., Sánchez, D., Torrella, E., 2015b. Experimental evaluation of an internal heat exchanger in a CO2 subcritical refrigeration cycle with gas-cooler. Applied Thermal Engineering 80, 31-41.
Moffat, R.J., 1985. Using Uncertainty Analysis in the Planning of an Experiment. Journal of Fluids Engineering 107, 173-178.
Nebot-Andrés, L., Calleja-Anta, D., Sánchez, D., Cabello, R., Llopis, R., 2019a. Thermodynamic analysis of a CO2 refrigeration cycle with integrated mechanical subcooling. Energies 13.
Nebot-Andrés, L., Llopis, R., Catalán-Gil, J., Sánchez, D., Calleja-Anta, D., Cabello, R., 2019b. Thermodynamics analysis of CO2 refrigeration cycles working with mechanical subcooling systems, 25th IIR International Congress of Refrigeration, Montreal, Canada.
Nebot-Andrés, L., Llopis, R., Sánchez, D., Catalán-Gil, J., Cabello, R., 2017. CO2 with mechanical subcooling vs. CO2 cascade cycles for medium temperature commercial refrigeration applications thermodynamic analysis. Applied Sciences (Switzerland) 7.
Sánchez, D., Catalán-Gil, J., Llopis, R., Nebot-Andrés, L., Cabello, R., Torrella, E., 2016. Improvements in a CO2 transcritical plant working with two different subcooling systems, Refrigeration Science and Technology, pp. 1014-1022.
Sarkar, J., Agrawal, N., 2010. Performance optimization of transcritical CO2 cycle with parallel compression economization. International Journal of Thermal Sciences 49, 838-843.
Sarkar, J., Bhattacharyya, S., Gopal, M.R., 2004. Optimization of a transcritical CO2 heat pump cycle for simultaneous cooling and heating applications. International Journal of Refrigeration 27, 830-838.
Shapiro, D., 2009. Refrigeration system with mechanical subcooling, https://patentimages.storage.googleapis.com/56/2a/72/a987f71d7ab41a/US7628027.pdf, United States.
Song, Y., Cao, F., 2018. The evaluation of the optimal medium temperature in a space heating used transcritical air-source CO2 heat pump with an R134a subcooling device. Energy Conversion and Management 166, 409-423.
Song, Y., Ye, Z., Wang, Y., Cao, F., 2018. The experimental verification on the optimal discharge pressure in a subcooler-based transcritical CO2 system for space heating. Energy and Buildings 158, 1442-1449.
Torrella, E., Sánchez, D., Llopis, R., Cabello, R., 2011. Energetic evaluation of an internal heat exchanger in a CO_2 transcritical refrigeration plant using experimental data. International Journal of Refrigeration 34, 40-49.
Yu, B., Yang, J., Wang, D., Shi, J., Chen, J., 2019. An updated review of recent advances on modified technologies in transcritical CO2 refrigeration cycle. Energy 189, 116147.

Table 4. Main experimental results and uncertainty measurements

	$t_{g,in}$ (ºC)	t_0 (ºC)	$t_{w,in}$ (ºC)	$p_{gc,o}$ (bar)	$t_{gc,o}$ (ºC)	SUB (ºC)	m_{CO2} (kg/s)	Pc_{main} (kW)	Pc_{ims} (kW)	Q_0 (kW)	$\varepsilon(Q_0)$ (kW)	$\varepsilon(Q_0)$ (%)	COP (-)	ε(COP) (-)	ε(COP) (%)		ΔQ_{evap} (%)	ΔQ_{gc} (%)	ΔQ_{sub} (%)
E1	-1.4	-15.6	25.2	74.5	27.5	21.3	0.03	3.36	0.77	7.71	0.05	0.66	1.87	0.015	0.78		-3.3	-2.5	4.4
E2	3.7	-11.2	25.0	74.7	28.1	17.8	0.04	3.47	0.72	8.91	0.06	0.73	2.13	0.018	0.84		-5.2	-3.0	3.3
E3	9.9	-5.9	24.8	74.6	29.2	12.5	0.05	3.53	0.61	10.28	0.09	0.87	2.48	0.024	0.97		-4.7	-4.9	6.6
E4	-1.3	-14.6	30.5	80.9	32.9	19.1	0.03	3.54	0.81	7.06	0.05	0.77	1.63	0.014	0.88		-2.8	-4.3	7.2
E5	3.8	-10.2	30.4	81.9	33.2	16.7	0.04	3.73	0.75	8.15	0.07	0.82	1.82	0.017	0.92		-1.8	-2.8	1.9
E6	9.9	-5.3	30.2	81.6	33.6	10.1	0.05	3.80	0.59	9.23	0.10	1.05	2.10	0.024	1.13		-6.4	-6.3	8.8
E7	-1.3	-14.5	35.0	88.4	36.1	20.6	0.03	3.72	0.90	6.49	0.05	0.76	1.40	0.012	0.86		-3.4	-3.2	5.7
E8	3.9	-9.8	35.2	89.8	36.9	14.6	0.04	3.95	0.74	7.34	0.07	0.92	1.56	0.016	1.01		-2.7	-2.7	3.4
E9	10.3	-4.1	35.1	89.4	37.5	8.9	0.05	4.12	0.61	8.55	0.11	1.25	1.81	0.024	1.32		-0.3	-4.1	5.2